J. Biochem. 129, 461–468 (2001)

Crystal Structure of *Bacillus stearothermophilus* α-Amylase: Possible Factors Determining the Thermostability[1]

Duvjir Suvd,*† Zui Fujimoto,† Kenji Takase,† Masatoshi Matsumura,* and Hiroshi Mizuno*†,[2]

Institute of Applied Biochemistry, University of Tsukuba, Tsukuba, Ibaraki 305-8572; and †Department of Biotechnology, National Institute of Agrobiological Resources, Tsukuba, Ibaraki 305-8602

Received November 2, 2000; accepted December 26, 2000

The crystal structure of a thermostable α-amylase from *Bacillus stearothermophilus* (BSTA) has been determined at 2.0 Å resolution. The main-chain fold is almost identical to that of the known crystal structure of *Bacillus licheniformis* α-amylase (BLA). BLA is known to be more stable than BSTA. A structural comparison between the crystal structures of BSTA and BLA showed significant differences that may account for the difference in their thermostabilities, as follows. (i) The two-residue insertion in BSTA, Ile181-Gly182, pushes away the spatially contacting region including Asp207, which corresponds to Ca^{2+}-coordinating Asp204 in BLA. As a result, Asp207 cannot coordinate the Ca^{2+}. (ii) BSTA contains nine fewer hydrogen bonds than BLA, which costs about 12 kcal/mol. This tendency is prominent in the $(\beta/\alpha)_8$-barrel, where 10 fewer hydrogen bonds were observed in BSTA. BLA forms a denser hydrogen bond network in the inter-helical region, which may stabilize α-helices in the barrel. (iii) A few small voids observed in the α-helical region of the $(\beta/\alpha)_8$-barrel in BSTA decrease inter-helical compactness and hydrophobic interactions. (iv) The solvent-accessible surface area of charged residues in BLA is about two times larger than that in BSTA.

Key words: α-amylase, *Bacillus stearothermophilus*, Ca^{2+}-binding, crystal structure, thermostability.

α-Amylase (α-1,4-glucan-4-glucanohydrolase, EC 3.2.1.1) catalyzes the hydrolysis of α-D-(1,4)-glucosidic linkages in starch and related carbohydrates, releasing α-anomeric products. To date, α-amylases from various sources have been isolated and characterized. The α-amylase from *Bacillus stearothermophilus* (BSTA) is a thermostable enzyme. Its amino acid sequence is homologous to those of *B. amyloliquefaciens* α-amylase (BAA) (66% sequence identity) and *B. licheniformis* α-amylase (BLA) (65% sequence identity), but there are significant differences in the thermostabilities of these amylases as follows. The half-lives of irreversible thermoinactivation at 90°C and pH 6.5 (pH optimum) are 2 min (BAA), 50 min (BSTA), and 270 min (BLA) (*1*); the temperature optima are 60, 75, and 90°C, respectively (*2*). The high degree of homology in their amino acid sequences suggests that their three-dimensional structures are also very similar. Since the crystal structure of BLA (but not that of BAA) is known (*3*), solving the structure of BSTA would enable us to examine the thermostability differences in terms of the differences in their three-dimensional structures. Recently, we successfully obtained crystals of recombinant wild-type BSTA suitable for X-ray diffraction analysis (*4*). In this paper we report the three-dimensional structure of BSTA. We compared the structures of BSTA and BLA with respect to overall topology, metal ion binding, hydrogen-bonding and hydrophobic interactions, and other molecular characteristics including accessible surface area and cavities. We discuss the results in relation to the thermostability difference between the two α-amylases. In particular, a two-residue insertion seen in BAA and another homologous α-amylase from *Bacillus* sp. KSM-1378 (LAMY), relative to BLA in sequence alignment, was previously shown by site-directed mutagenesis to be a cause of the thermal instability (*5*, *6*). BSTA also has the same insertion and we provide a structural basis for the effect of the insertion on thermostability.

MATERIALS AND METHODS

Enzyme Preparation and Crystallization—The recombinant α-amylase from *B. stearothermophilus* A631 was produced in the *B. subtilis* expression system, and several isoforms were purified from the culture supernatant as described previously (*4*, *7*). A pI 8.2 isoform formed tiny needle crystals under the following conditions: 35 mM Na-acetate (pH 4.6), 35 mM $CaCl_2$, 6.25% (v/v) 2-propanol, in the presence of 1.23% (w/v) acarbose (a pseudo-oligosaccharide inhibitor, kindly provided by Bayer as a gift) in the drop at a protein concentration of 10 mg/ml. X-ray intensity data were collected at the BL-6A station of the Photon Fac-

[1] This work was supported in part by a grant to the Rice Genome Project PR-2106, MAFF, Japan, and performed with the approval of the Photon Factory Advisory Committee, the High Energy Accelerator Research Organization, Japan (Proposal number 98G157).

[2] To whom correspondence should be addressed. Phone: +81-298-38-7014, Fax: +81-298-38-7408, E-mail: mizuno@abr.affrc.go.jp

Abbreviations: ASA, accessible surface area; BAA, α-amylase from *Bacillus amyloliquefaciens*; BLA, α-amylase from *Bacillus licheniformis*; BSTA, α-amylase from *Bacillus stearothermophilus*; LAMY, α-amylase from *Bacillus* sp. KSM-1378; RMS, root mean square.

tory using the Weissenberg camera (*8*). Data were processed with the program DENZO and merged using the program SCALEPACK (*9*, Table I).

Structure Determination—The structure of BSTA was determined by the molecular replacement method using the program AMoRe (*10*) in the CCP4 suite (*11*). The structure of BLA (1bpl; Protein Data Bank entry) was used as the initial reference model. Both the rotation- and translation-function searches gave a single solution. The translation function had a correlation coefficient of 0.41 and an *R*-factor of 0.450 in the 6–3.0 Å resolution range. After rigid-body refinement, which resulted in an *R*-factor of 0.424 in the 6–2.5 Å resolution range, the iterative process of positional and simulated annealing refinement was followed using the program X-PLOR (*12*) with the parameters of Engh and Huber (*13*). Ten percent of the observed reflections were randomly removed for the cross-validation (*14*). Coordinates were adjusted repeatedly against the renewed $2F_{obs}$–F_{calc} and F_{obs}–F_{calc} electron density maps with the program QUANTA (Molecular Simulations). During the course of refinement, three Ca^{2+} ions and one Na^{+} ion were identified for the large peaks in the difference Fouriers map. Solvent molecules were identified as positive peaks in electron density maps within hydrogen-bonding distance of appropriate protein atoms or other solvent atoms. The quality of the structure was analyzed using the programs WHATIF (*15*) and PROCHECK (*16*). The results of analysis are summarized in Table I. The coordinates for BSTA were deposited in the RCSB Protein Data Bank (accession number 1hvx).

Structural Comparison—The coordinate of BLA was obtained from the RCSB Protein Data Bank (accession number 1bli), which contained the mutations N190F, Q264S, and N265Y. Structural comparison was conducted with the program QUANTA. Accessible surface areas (ASA) were calculated using the program GRASP (*17*). Cavities were sought using the program VOIDOO (*18*) on both proteins using a number of different parameters and protein orientations. We also used the program VOIDOO to calculate the packing densities (the ratio of the van der Waals volume of an atom to the actual space it occupies (*19*)). The real volumes were calculated by the Voronoi procedure (*20*) using the programs ACCESS and VOLUME (*21*).

TABLE I. **Crystal parameters and refinement statistics.**

Space group	$P2_1$
Cell parameters (Å, °)	a=53.5 b=92.8 c=53.1, β=109.4
Solvent content (%)	41
Resolution range (Å)	8.0–2.0
No. of reflections in refinement	28,367
R-factor[a]	0.156
R_{free}-factor[b]	0.197
No. of protein atoms	3,909
No. of metal atoms	4
No. of water molecules	320
Average *B*-factor (Å^2)	9.6
Protein atoms (Å^2)	9.1
Metal ions (Å^2)	5.7
Solvent atoms (Å^2)	18.6
RMS deviations	
from ideal bond lengths (Å)	0.008
from ideal bond angles (°)	1.4
from ideal dihedral angles (°)	24.2

[a]*R*-factor is defined as $R = \Sigma ||F_{obs}| - |F_{calc}|| / \Sigma |F_{obs}|$. [b]$R_{free}$-factor was calculated using 10% of the unique reflections.

RESULTS AND DISCUSSION

Quality of the Model—The quality of the structure was assessed using the program PROCHECK (*16*) and WHATIF (*15*). In the Ramachandran plot (*22*), 87.4% of non-glycine residues have their backbone torsion angles in the most favoured region and 11.8% residues in the additional allowed region. Only one residue Tyr151 (ϕ = 83°, ψ = −40.5°) lay in the disallowed area, although it has a well-defined electron density map. In the omit map, where Tyr-151 and neighboring residues were omitted from the model, the difference electron density confirmed their correct placement. The mean positional error of the atoms as estimated from the Luzatti plot (*23*) is 0.21 Å. Crystal parameters and refinement statistics are listed in Table I. Among the residues from −2 to 515 deduced from the DNA sequence (*24*) and N-terminal amino acid sequence analysis (*4*), residues 1–483 were visible in the electron density maps, but the remaining residues were not, probably because of their disordered structure. Acarbose, a substrate analogue inhibitor is not visible at the active site in the electron density maps, although it was added during crystallization (*4*). The final model resulted in an *R*-factor of 0.156 and an R_{free}-factor of 0.197 in the resolution range of 8.0–2.0 Å. The average of *B*-factors is 9.6 Å^2 for all atoms and 9.1 Å^2 for protein atoms. These unusually low values are consistent with the fact that the crystals diffracted beyond 2.0 Å resolution considering the very small crystals with maximum dimensions of 0.1 × 0.05 × 0.02 mm (*4*).

The Overall Structure of BSTA—BSTA consists of a single polypeptide chain, folded into three distinct domains A, B, and C, as commonly observed in α-amylases (Figs. 1 and 2). Domain A represents a compact core structure comprising a $(\beta/\alpha)_8$-barrel. Domain B shows a variable structure among α-amylases. It is composed of a sheet of four antiparallel β-strands with a pair of antiparallel β-strands, with fairly long loops between β-strands. The Ca^{2+}-Na^{+}-Ca^{2+} binding site is located in the interior of domain B, spanning to the interface with domain A, as described later. Domain C forms a distinct globular unit consisting of eight β-strands folded into a Greek key motif, and forms the third Ca^{2+} binding site in cooperation with domain A (Fig. 1).

Figure 3 shows a superposition with BLA. The root mean square (RMS) difference for Cα atom pairs is 0.83 Å. The residues involved in the secondary structure elements (α-helices and β-strands) are shown in the topological alignment of the enzymes (Fig. 2). The main secondary structural elements are essentially the same in both enzymes. The two amylases display 65% amino acid sequence identity. Of the 35% total difference (169 residues) between the two amylases, 37% (63 residues) are in α-helices.

Active Site—The active site is located on the C-terminal side of the β-strands of the $(\beta/\alpha)_8$-barrel in domain A. From the structural comparison with other α-amylases, Asp234, Glu264, and Asp331 are assigned as the catalytic residues in BSTA (Fig. 2). The residues in the active site are strictly conserved, but some positional differences are observed when superimposed with BLA, particularly in the catalytic residues. This may reflect the flexible nature of catalytic residues, which may be important for catalytic reactions.

The structure of the active site is also similar to that of

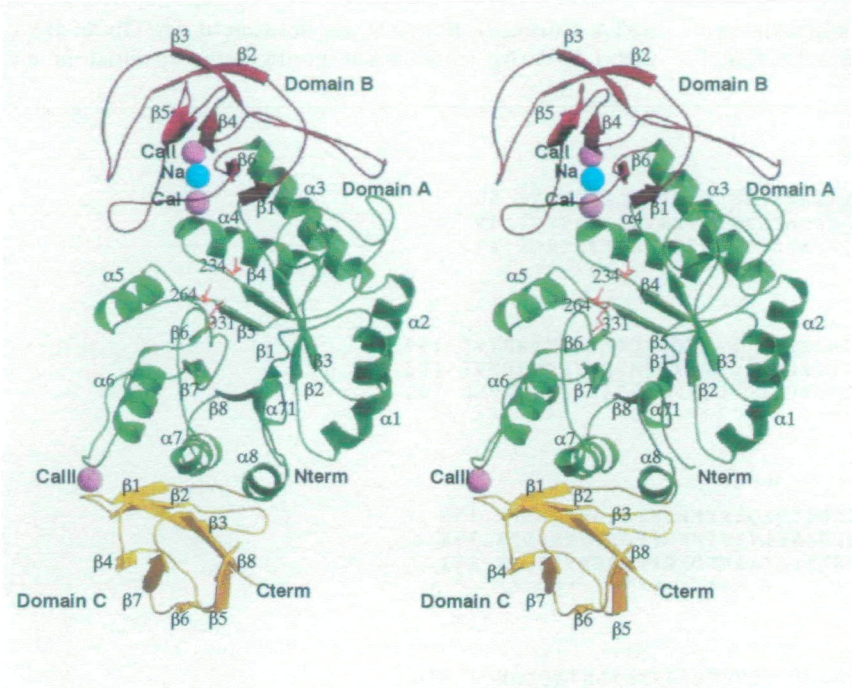

Fig. 1. **Stereoview of a ribbon model of BSTA.** This model was generated with the program MOLSCRIPT (*33*). Metal ions are shown as spheres. Active site residues are numbered and shown in liquorice. Domains are shown in different colors.

Taka-amylase A, which rationalizes the mutant designs previously made by us (*7*) to investigate the effect of mutations near the catalytic site. In the previous design we referred to the structure of Taka-amylase A (*25*) and found that Asn295 (Asn329 in BSTA) is located in close proximity (4–5 Å distance between side-chain atoms) to Asp297 (Asp-331 in BSTA), one of the catalytic residues. The current structure of BSTA shows that the corresponding residues in BSTA are arranged in similar positions. In the previous study we mutated Asn329 to Lys, Asp, and Val, resulting in altered specific activity, and changes in the pH and temperature dependence of activity (*7*). Noteworthy is the Asp-329→Val mutant that showed much higher activity than the wild-type enzyme at low temperatures (5–15°C). We modeled the structures of these mutants and found that they do not deviate much from the wild-type structure. Thus, the mutated residues are close to Asp331 so that they can affect the catalytic activity. This validates our previous interpretation that the altered catalytic properties of the mutant enzymes are the results of the charge or hydrophobic effects of the mutated residues on Asp331.

The Metal Ion Binding Sites—In the course of refinement, three peaks with a high level of electron density appeared in the interior of domain B and another at the interface between domain A and domain C. These peak positions correspond to those of three Ca^{2+} and one Na^{+} in BLA (*3*), and are therefore shown as CaI, CaII, CaIII, and Na in Figs. 1 and 2.

CaI is strictly conserved in all α-amylases. CaI and CaII form a linear triad with a sodium ion as described in BLA, but there are some differences between the two α-amylases, as follows. (i) The side-chain OD1 of Asp204 in BLA is involved in the binding of CaII, but the side chain of the corresponding residue Asp207 in BSTA is positioned away from binding to CaII. Instead, a water molecule participates in coordinating CaII (Fig. 4a). (ii) Asn104 in BLA is replaced by Asp105 in BSTA, but both residues are involved in the coordination to CaI.

CaIII contributes to bridging between two loops, one of which comes from Aα6 of domain A and the other protrudes between Cβ1 and Cβ2 of domain C (Fig. 4b). There are some differences in the coordinating residues to CaIII: Tyr302 in BLA is replaced by Phe305 in BSTA and His406 in BLA by Ser406 in BSTA.

Interpretation of the Thermostability Difference Based on Structural Comparison with BLA—The nature of the thermostability of various enzymes has been extensively investigated. Although certain criteria stand for the thermostability of proteins in general, it appears that the thermostability of a particular enzyme is a reflection of its unique structure. Here we compare the structures of BSTA and BLA and discuss their thermostability difference.

The superposition of the Cα-models (Fig. 3) and the topological alignment (Fig. 2) of BSTA and BLA show that the length and position of individual secondary structural elements are almost identical in both enzymes. Moreover, as shown in Table II, the total solvent accessible surface area, volume, and molecular packing densities of both molecules are very similar. The total void volumes of both BSTA and BLA are very small in general compared with other protein molecules. Thus, it is difficult to account for the thermostability difference on the basis of the overall structure. It is likely that the thermostability difference can be ascribed to the local structural environment.

BSTA has four very short insertions and deletions of 1 to 2 residues in the amino acid sequence as compared to BLA (Fig. 2). The two-residue insertion in BSTA, Ile181-Gly182, pushes away the spatially contacting region, including Asp207, which corresponds to Ca^{2+}-coordinating Asp204 in BLA. As a result, the side-chain of Asp207 cannot coordinate CaII, although a water molecule contributes to the restoration of the CaII coordination geometry (Fig. 5). BAA and a semi-alkaline α-amylase LAMY also possess the two-residue insertion at exactly the same position as in BSTA: Glu178-Gly179 in BAA (Fig. 2) and Thr183-Gly184 in LAMY (*5*, *6*). Previously, when the three-dimensional structures of none of these α-amylases were known, Suzuki *et al.* (*5*) and Igarashi *et al.* (*6*) erroneously regarded the inser-

tion as Arg179-Gly180 (BSTA numbering), which is two residues upstream and conserved among BAA, LAMY, and BSTA. Curiously, however, the deletion of Arg-Gly in BAA and LAMY by site-directed mutagenesis resulted in an

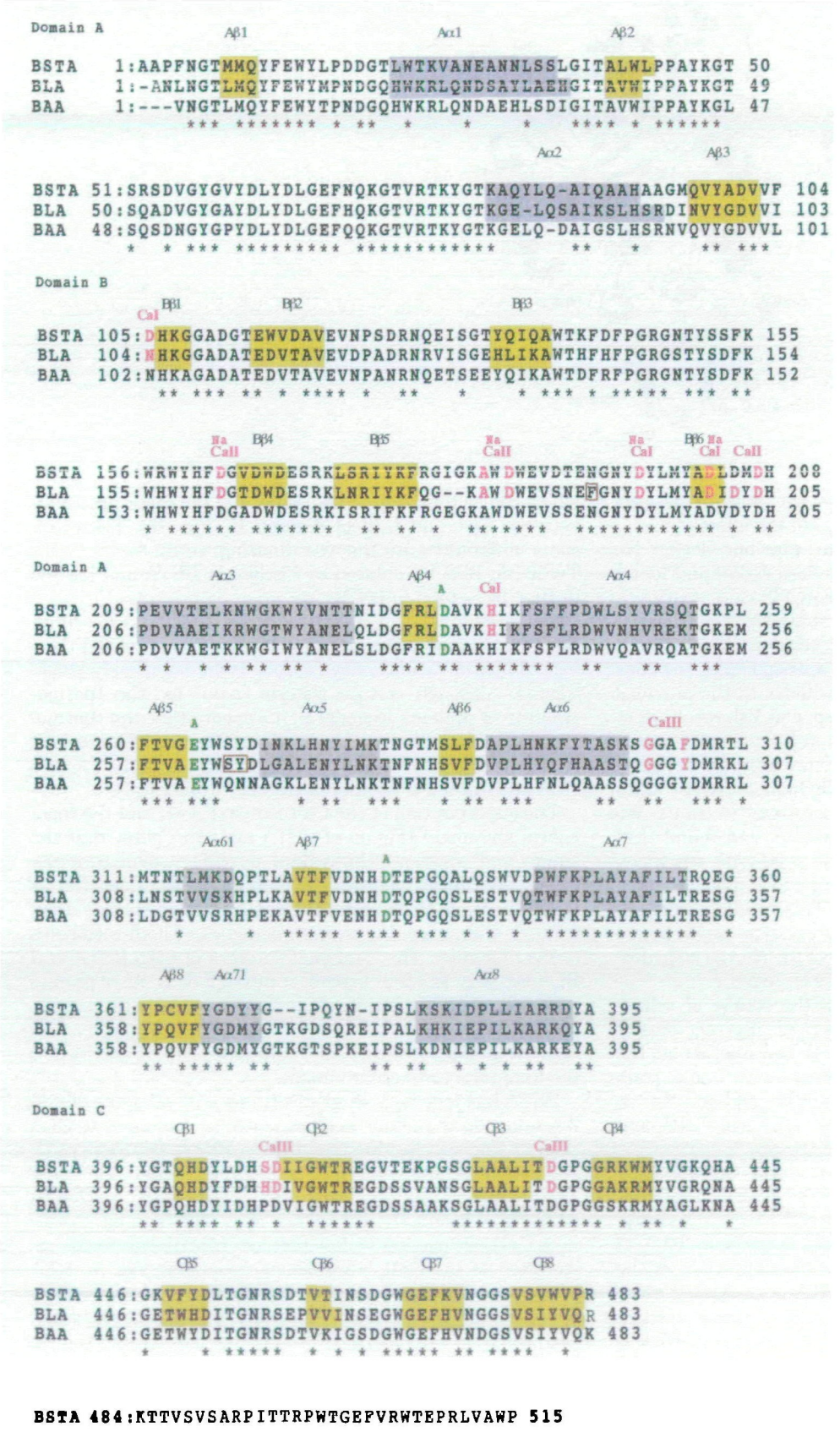

Fig. 2. **Topological alignment of BSTA and BLA (variant containing the mutations N190F, Q264S, and N265Y as shown in dark brown boxes) along with the amino acid sequence alignment of BAA.** The alignment is based on the superimposed models. Residues that belong to α-helices and β-strands are marked in blue and yellow, respectively. Residues involved in calcium and sodium ion binding sites are indicated by *CaI*, *CaII*, CaIII, and Na, respectively. The catalytic-site residues are indicated by the letter A in green. Secondary structural elements are named. Conserved amino acids are marked with asterisks. Residues not determined by X-ray studies are written in thin letters.

Fig. 3. **Stereoview of superimposed Cα-models of BSTA (red) and BLA (gray).** BSTA is numbered every 20 residues.

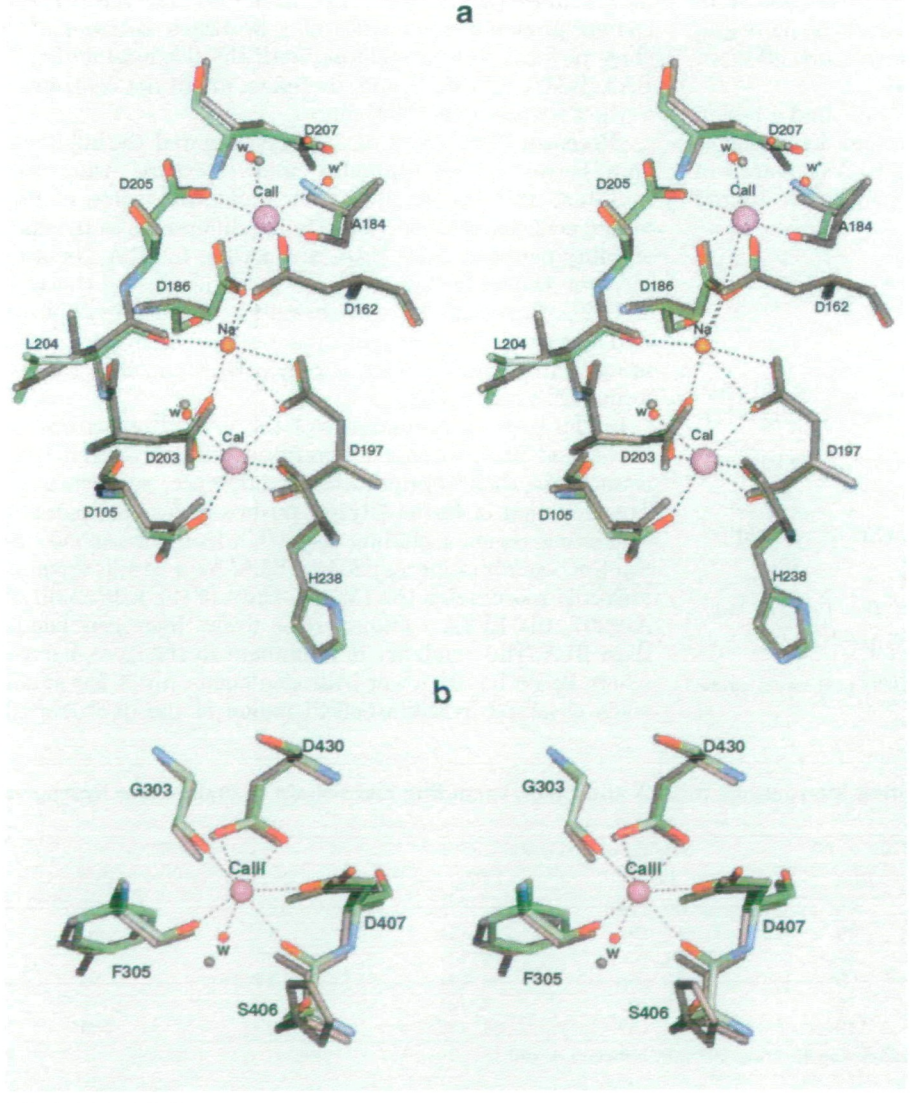

Fig. 4. **Stereoview of the superposition of the amino acid residues involved in metal-binding in BSTA (shown by element; atoms are colored in: C- green, N- blue, and O- red) and in BLA (gray).** Water molecules (w) are shown as small spheres. A water molecule involved in CaII-binding in BSTA is marked with an asterisk: (a) CaI-Na-CaII triad; (b) CaIII.

increase in thermostability. Apparently, the deletion of either Arg-Gly or the next two residues downstream, the actual insertion site, removes the bulge created by the two extra residues (Fig. 5), and thus seems to have similar consequences on the thermostability by affecting CaII binding. However, Arg179 in BSTA forms a salt bridge with Glu129 (Fig. 5), which may contribute to thermostability. Therefore, the deletion of Ile181-Gly182 rather than Arg179-Gly180 is expected to result in a higher thermostability. We predict a similar enhancement of thermostability by deleting the actual insertion rather than Arg-Gly for BAA and LAMY. Site-directed mutagenesis of this region in BSTA is currently under way in our laboratory.

Table III shows the total number of hydrogen bonding interactions in each domain of BSTA and BLA, where the numbers of hydrogen bonding interactions between main-chain and side-chain atoms and between side-chain and side-chain atoms are simply compared between BSTA and BLA. In total, BSTA has nine fewer hydrogen bonds than BLA, which costs about 12 kcal/mol (*26*). This tendency is prominent in domain A comprising the $(\beta/\alpha)_8$-barrel, where 10 more hydrogen bonds are observed in BLA, forming a denser hydrogen bond network in the inter-helical region of the $(\beta/\alpha)_8$-barrel, which may stabilize α-helices in the barrel. On the other hand, in domain B, BSTA has six more hydrogen bonds (including four more salt bridges) than BLA. Therefore, domain B of BSTA appears to be more stable than that of BLA, but this may not have much effect on the thermostability of the entire molecule.

By careful inspection of the structures, we found a region that differs in local hydrogen bonding and hydrophobic stacking interactions between BSTA and BLA as shown in Fig. 6, (a) and (b). BLA forms 16 hydrogen bonds around Aα1, Aα2, and Aα8. Gln20, Lys23, Arg24 in Aα1 and Glu82 in Aα2 of BLA are replaced by Thr21, Thr24, Lys25, and Gln83 in BSTA, respectively, resulting in the loss of seven hydrogen bonds. A hydrophobic core is observed in BLA between four tyrosine rings (Tyr10, Tyr31, Tyr363, and Tyr367) and hydrophobic residues from Aα8, Aα1, Aα2, Aβ2, and Aβ3. The corresponding region in BSTA generates two small contiguous voids (Fig. 6a, arrows) with a total volume of 26 Å^3 that are obviously derived from the change of residues Asp28, Tyr31, Leu90, and Met366 in BLA to Lys25, Asn32, Ala91, and Tyr369 in BSTA. The local differences in this region may contribute to the thermostability difference between BSTA and BLA.

As seen from the data in Table II, the percentage of the total accessible surface area (ASA) comprising charged residues in BLA is about two times greater than in BSTA. Histidine residues contribute largely to this difference, because BLA has 13 more histidines than BSTA, of which seven histidines replace hydrophobic residues partially exposed in BSTA, assuming Tyr to be a hydrophobic residue. The remaining six histidine residues are replaced by polar residues. Since hydration of nonpolar groups apparently destabilizes proteins (*27*), the above substitutions may contribute in part to the stabilization of BLA.

Criteria such as the number of Asn and Gln (*28*) or Pro (*29*) residues, the Arg/Arg+Lys ratio (*30*), and the helices-content/protein-content ratio of β-branched residues (*31*) show no significant correlation with the thermostability of BAA, BSTA, and BLA, and, therefore, might not contribute to the thermostability differences.

Recently, Declerck *et al.* (*32*) investigated the relationship between thermostability and structure using the mutation analysis of BLA, and found that some of the amino acid changes contribute to the differences in thermostability between BLA, BAA, and BSTA. In BLA, replacement of Ala269 by Lys caused a reduction in the thermostability. However, the corresponding residue, Lys272, in BSTA may not be destabilizing because it forms a salt bridge with Asp190, which is Ser in BLA and thus cannot form such a salt bridge.

In the present comparison of the crystal structures of BSTA and BLA, we found significant differences that may account for their thermostability difference, as follows. (i) The insertion of Ile181-Gly182 pushes away the spatially contacting region including Asp207, which corresponds to the Ca^{2+}-coordinating Asp204 in BLA. As a result, a water molecule coordinates the Ca^{2+} in place of the side chain of Asp207. (ii) BSTA contains nine fewer hydrogen bonds than BLA. This tendency is prominent in the $(\beta/\alpha)_8$-barrel, where BSTA has 10 fewer hydrogen bonds. (iii) A few small voids observed in the α-helical region of the $(\beta/\alpha)_8$-barrel

TABLE II. **Accessible surfaces, cavities, and volumes.**

	BSTA	BLA
Total solvent accessible surface area (ASA; Å^2)	17,479	17,388
Total (% of total) ASA of polar residues	5,133 (29)	5,081 (29)
Total (% of total) ASA of hydrophobic residues	2,214 (12.7)	2,141 (12)
Total (% of total) ASA of charged residues	2,645 (15)	4,899 (28)
Volumes and voids (Å^3):		
Volume of molecules	88,470	87,930
Total void volumes[a]	46	18
Molecular packing densities	1.17	1.19
Hydrophobic residues	Ala, Ile, Leu, Met, Phe, Pro, Trp, Val	
Polar residues	Ser, Gln, Asn, Gly, Thr, Cys, Tyr	
Charged residues	Asp, Arg, Glu, His, Lys	

[a]Voids were detected with the program VOIDOO (*18*) using probe radius 1.5 Å and atom fattening factor 1.09.

TABLE III. **The number of hydrogen bonding interactions in BLA and BSTA, excluding main-chain to main-chain hydrogen bonds.**

Hydrogen bonds	Main-chain to side-chain atoms		Side-chain to side-chain atoms		Total	
	BSTA	BLA	BSTA	BLA	BSTA	BLA
Domain A	81	80	40 (18)[a]	51 (18)	121	131
Domain B	29	30	17 (9)	10 (5)	46	40
Domain C	26	30	14 (3)	14 (3)	40	44
Domain A/B[b]	4	5	10 (5)	9 (4)	14	14
Domain A/C[c]	4	4	2 (0)	3 (2)	6	7
Total	144	149	83 (35)	87 (32)	227	236

[a]Number of salt bridges. [b]Inter-domain between A and B. [c]Inter-domain between A and C.

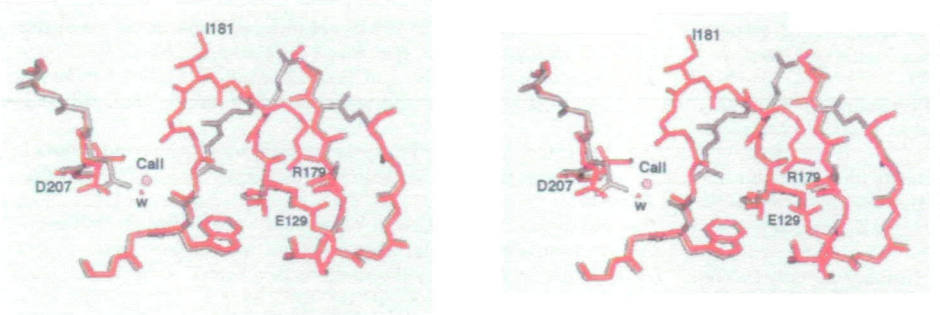

Fig. 5. **Stereoview of the superposition of the area of the two amino acid residue insertion (Ile181-Gly182) over BLA.** BSTA is drawn in red and BLA in gray. A calcium ion is drawn as a pink sphere, and a water molecule as a red sphere. Residues are labeled according to BSTA.

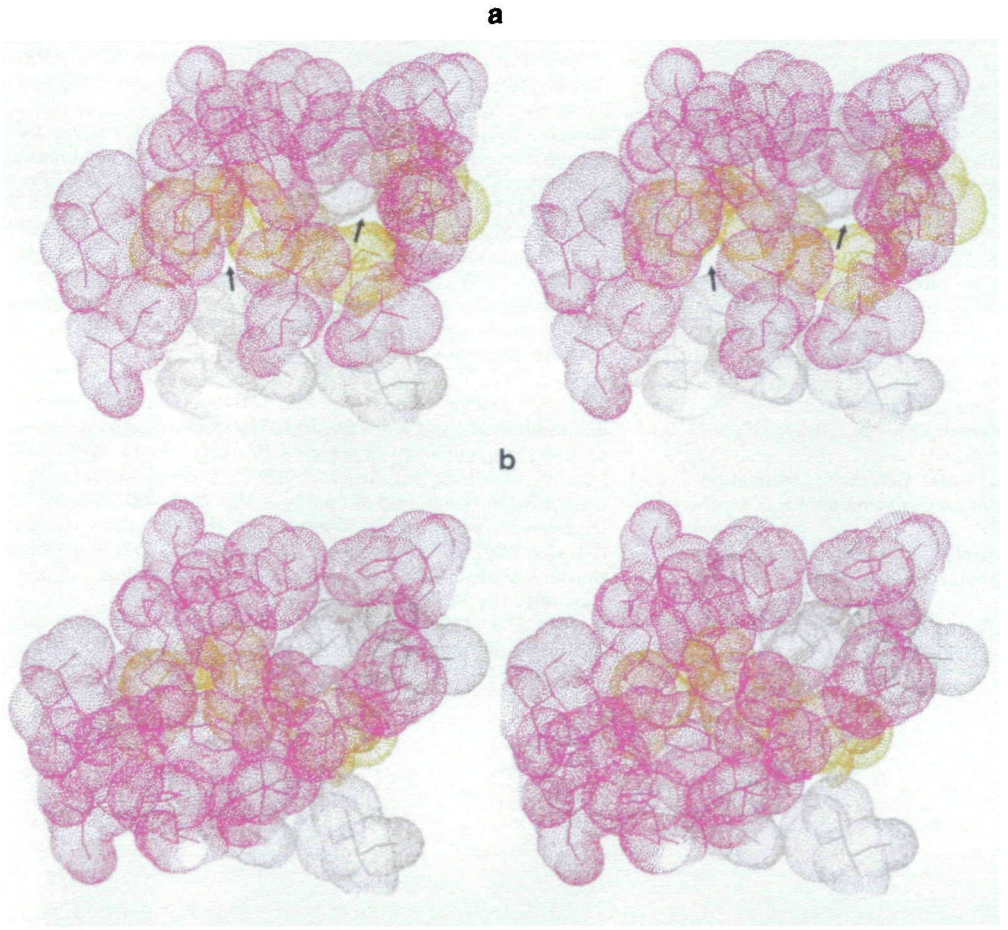

Fig. 6. **Stereoview of van der Waals drawings around Aα1, Aα2, Aα8, Aβ2, and Aβ3 in BSTA (a) and BLA (b).** Residues and dot surfaces are shown in different colors with α-helices in purple, β-strands in yellow, and loops in gray. Voids in BSTA are indicated by arrows.

domain in BSTA decrease inter-helical compactness and hydrophobic interactions. (iv) The percentage of solvent-accessible surface area of charged residues in BLA is about two times larger than that in BSTA.

We wish to thank Prof. N. Sakabe and Drs. N. Watanabe, M. Suzuki, and N. Igarashi of the Photon Factory, High Energy Accelerator Research Organization, for their help in data collection using the Weissenberg camera and synchrotron radiation.

REFERENCES

1. Tomazic, S.J. and Klibanov, A.M. (1988) Mechanisms of irreversible thermal inactivation of *Bacillus* α-amylases. *J. Biol. Chem.* **263**, 3086–3091
2. Vihinen, M., Ollikka, P., Niskanen, J., Meyer, P., Suominen, I., Karp, M., Holm, L., Knowles, J., and Mäntsälä, P. (1990) Site-directed mutagenesis of a thermostable α-amylase from *Bacillus stearothermophilus*: putative role of three conserved residues. *J. Biochem.* **107**, 267–272
3. Machius, M., Declerck, N., Huber, R., and Wiegand, G. (1998) Activation of *Bacillus licheniformis* α-amylase through a disorder → order transition of the substrate-binding site mediated by a calcium-sodium-calcium metal triad. *Structure* **6**, 281–292
4. Suvd, D., Takase, K., Fujimoto, Z., Matsumura, M., and Mizuno, H. (2000) Purification, crystallization and preliminary X-ray crystallographic study of α-amylase from *Bacillus stearothermophilus*. *Acta Cryst.* **D56**, 200–202
5. Suzuki, Y., Ito, N., Yuuki, T., Yamagata, H., and Udaka, S. (1989) Amino acid residues stabilizing a *Bacillus* α-amylase against irreversible thermoinactivation. *J. Mol. Biol.* **264**, 18933–18938
6. Igarashi, K., Hatada, Y., Ikawa, K., Araki, H., Ozawa, T., Kobayashi, T., Ozaki, K., and Ito, S. (1998) Improved thermostability of an arginine-glycine residue is caused by enhanced calcium binding. *Biochem. Biophys. Res. Commun.* **248**, 372–377
7. Takase, K. (1993) Effect of mutation of an amino acid residue near the catalytic site on the activity of *Bacillus stearothermophilus* α-amylase. *Eur. J. Biochem.* **211**, 899–902
8. Sakabe, N. (1991) X-ray diffraction data collection system for

modern protein crystallography with a Weissenberg camera and an imaging plate using synchrotron radiation. *Nucl. Instrum. Methods Phys. Res.* **A303**, 448–463
9. Otwinowski, Z. and Minor, W. (1997) Processing of X-ray diffraction data collected in oscillation mode. *Methods Enzymol.* **276**, 307–326
10. Navaza, J. (1992) AMoRE: a new package for molecular replacement in *Molecular Replacement* (Dodson, E.J., Gover, S., and Wolfe, W., eds.) pp. 87–90, Daresbury Laboratory, Warrington, UK
11. Collaborative Computational Project, Number 4 (1994) The CCP4 Suite: Programs for protein crystallography. *Acta Cryst.* **D50**, 760–763
12. Brünger, A.T., Kuriayan, J., and Karplus, M. (1987) Crystallographic *R* factor refinement by molecular dynamics. *Science* **235**, 458–460
13. Engh, R.A. and Huber, R. (1991) Accurate bond and angle parameters for X-ray protein structure refinement. *Acta Cryst.* **A47**, 392–400
14. Brünger, A.T. (1992) Free *R* value: a novel statistical quantity for assessing the accuracy of crystal structures. *Nature* **355**, 472–475
15. Vriend, G. (1990) WHAT IF: A molecular modeling and drug design program. *J. Mol. Graph.* **8**, 52–56
16. Laskowski, R.A., MacArthur, M.W., Moss, D.S., and Thornton, J.M. (1992) *PROCHECK v.2: Programs to Check the Stereochemistrial Quality of Protein Structures*, Oxford Molecular Ltd., Oxford, England
17. Anthony, N., Sharp, K.A., and Honig, B. (1991) Protein folding and association: insights from the interfacial and thermodynamic properties of hydrocarbons. *Proteins. Struct. Funct. Genet.* **11**, 281–296
18. Kleywegt, G.J. and Jones, T.A. (1994) Detection, delineation, measurement and display of cavities in macromolecular structures. *Acta Cryst.* **D50**, 178–185
19. Richards, F.M. (1974) The interpretation of protein structures: total volume, group volume distributions and packing density. *J. Mol. Biol.* **82**, 1–14
20. Voronoi, G.F. (1908) Nouvelles applications des paramètres continus à la théorie des formes quadratiques. *J. Reine Angew. Math.* **134**, 198–287
21. Richards, F.M. (1977) Areas, volumes, packing density and protein structure. *Annu. Rev. Biophys. Bioeng.* **6**, 151–175
22. Ramachandran, G.N. and Sasisekharan, V. (1968) Conformation of polypeptides and proteins. *Adv. Protein Chem.* **23**, 283–437
23. Luzzati, P.V. (1952) Traitement statistique des erreurs dans la determination des structures cristallines. *Acta Cryst.* **5**, 802–810
24. Sohma, A., Fujita, T., and Yamane, K. (1987) Protein processing to form extracellular thermostable α-amylases from a gene fused in a *Bacillus subtilis* secrection vector. *J. Gen. Microbiol.* **133**, 3271–3277
25. Matsuura, Y., Kusunoki, M., Harada, W., and Kakudo, M. (1984) Structure and possible catalytic residues of Taka-amylase A. *J. Biochem.* **95**, 697–702
26. Shirley, B.A., Stanssens, P., Hahn, U., and Pace, C.N. (1992) Contribution of hydrogen bonding to the conformational stability of ribonuclease T_1. *Biochemistry* **31**, 725–732
27. Spassov, V.Z., Karshikoff, A.D., and Ladenstein, R. (1995) The optimization of protein-solvent interactions: thermostability and the role of hydrophobic and electrostatic interactions. *Protein Sci.* **4**, 1516–1527
28. Klibanov, M.A. and Ahern, J.T. (1985) The mechanism of irreversible enzyme inactivation at 100°C. *Science* **228**, 1280–1284
29. Matthews, B.W., Nicholson, H., and Becktel, W.J. (1987) Enhanced protein thermostability from site-directed mutations that decrease the entropy of unfolding. *Proc. Natl Acad. Sci. USA* **84**, 6663–6667
30. Mrabet, N.T., Van den Broeck, A., Van den brande, I., Stanssens, P., Laroche, Y., Lambeir, A.M., Matthiijssens, G., Jenkins, J., Chiadmi, M., and van Tilbeurgh, H. (1992) Arginine residues as stabilizing elements in proteins. *Biochemistry* **31**, 2239–2253
31. Vogt, G., Woell, S., and Argos, P. (1997) Protein thermal stability, hydrogen bonds, and ion pairs. *J. Mol. Biol.* **269**, 631–643
32. Declerck, N., Machius, M., Wiegand, G., Huber, R., and Gaillardin, C. (2000) Probing structural determinants specifying high thermostability in *Bacillus licheniformis* α-amylase. *J. Mol. Biol.* **301**, 1041–1057
33. Kraulis, P.J. (1991) MOLSCRIPT: a program to produce both detailed and schematic plots of protein structures. *J. Appl. Cryst.* **24**, 946–950